Proceedings of ASME Turbo Expo 2011
GT2011
June 6-10, 2011, Vancouver, British Columbia, Canada

GT2011-46195

AUTOIGNITION LIMITS OF HYDROGEN AT RELEVANT REHEAT COMBUSTOR OPERATING CONDITIONS

Julia Fleck, Peter Griebel, Adam M. Steinberg, Michael Stöhr, Manfred Aigner
German Aerospace Center (DLR)
Institute of Combustion Technology
Pfaffenwaldring 38-40, 70569 Stuttgart, Germany
e-mail: Julia.Fleck@DLR.de

Andrea Ciani
ALSTOM Power Ltd.
Brown-Boveri-Strasse 7, 5400 Baden, Switzerland

ABSTRACT

The use of highly reactive fuels in the lean premixed combustion systems employed in stationary gas turbines can lead to many practical problems, such as unwanted autoignition in regions not designed for combustion. In the present study, autoignition characteristics for hydrogen, diluted with up to 30 vol. % nitrogen, were investigated at conditions relevant to reheat combustor operation (p = 15 bar, T > 1000 K, hot flue gas, relevant residence times). The experiments were performed in a generic, optically accessible reheat combustor, by applying high-speed imaging and Particle Image Velocimetry (PIV). Autoignition limits for different mixing section (temperature, velocity) and fuel jet (N_2 dilution) parameters are described. The dominant factor influencing autoignition was the temperature, with an increase of around 2% leading to a reduction of the highest possible H_2 concentration without "flame-stabilizing autoignition kernels" of approximately 16 vol. %. Furthermore, the onset and propagation of the ignition kernels were elucidated using the high-speed measurements. It was found that the ability of individual autoignition kernels to develop into stable flames depends on the initial position of the kernel and the corresponding axial velocity at that position. While unwanted autoignition occurred prior to reaching the desired operating point for most investigated conditions, for certain conditions the reheat combustor could be operated stably with up to 80 vol. % H_2 in the fuel.

Keywords: Autoignition, hydrogen, reheat combustion concept, high-speed imaging

INTRODUCTION

The demand for reduced CO_2 emissions has led to an increased interest in low-carbon fuels. Such hydrogen-rich fuels may be derived from the gasification of coal or biomass and are characterized by increased reactivity compared to natural gas (NG). Employing such highly reactive fuels in gas turbine (GT) lean premixed combustion systems, which are currently used to achieve stringent low emission targets, influences operability issues such as combustion stability, flashback and autoignition [1].

One concept differing from other lean premixed combustion systems can be found in ALSTOM®'s GT24® and GT26® family[1] [2, 3]. In this sequential combustion, or reheat concept, two combustion chambers are arranged in series. The first combustor is followed by a high pressure turbine stage, after which the flue gas is mixed with additional fuel and "reheated" in the second or reheat combustor. The flue gas is subsequently expanded in the low-pressure turbine. In the mixing zone leading into the reheat combustor, fuel is injected into exhaust gas at temperatures higher than 1000 K. To ensure safe

[1] ALSTOM® is a registered trademark; GT24®, GT26® are registered trademarks of ALSTOM Technology Ltd.

operation, autoignition must not occur in the mixing zone. Hence, knowing autoignition characteristics of highly reactive fuels at reheat combustor relevant operating conditions is essential for a proper design of the mixing zone.

Autoignition is a spontaneous process wherein a flammable mixture ignites and burns without the presence of an external ignition source. The time between the formation of a reactive mixture and the onset of chemical reactions is the ignition delay time, τ_{ign}. This parameter is a function of temperature, pressure, and gas composition, and is commonly measured under homogeneous conditions such as in shock tube devices or rapid compression machines. In such situations, τ_{ign} is mainly controlled by chemical kinetics. The results of such experiments provide a database to develop mechanisms for the prediction of ignition delay times. For hydrogen, a literature overview by Mittal et al. [4] reveals that few studies have been carried out at elevated pressures relevant for GTs. These have recently been supplemented by Refs. [5] and [6]. Herzler and Naumann [5] performed shock tube studies with H_2 and H_2 mixed with different amounts of an NG-like CH_4 blend at pressures of 1, 4 and 16 bar, temperatures between 900-1400 K, and equivalence ratios (Φ) of 0.5 and 1. At a pressure of 16 bar, ignition delay times of H_2 were found to be nearly independent of the equivalence ratio.

In practical systems, the additional influence of turbulence and mixing on the ignition delay must be considered. The mixing time of current low emission combustor premixers ranges up to 5 ms [7], which is sufficiently short to avoid autoignition for methane, ethane, and propane [8]. However, H_2 exhibits significantly shorter ignition delay times, especially for temperatures higher than 1000 K, so that ignition might occur during the mixing process.

Non-premixed ignition has been the subject of numerous previous studies. In a counterflow configuration between streams of hydrogen and preheated air, Kreutz and Law [9] found ignition to appear as a localized kernel near the maximum temperature. In an extensive review on turbulent non-premixed ignition [10], Mastorakos mentions that autoignition is preferentially located at the most reactive mixture fraction, which depends on the operating conditions and is found on the fuel lean side for H_2.

Besides mixing, the strain rate and the turbulence intensity were found to influence ignition [9, 11-13]. Blouch and Law [12] investigated the effects of turbulence intensity for a non-premixed cold hydrogen/nitrogen mixture ignited by heated air at pressures up to 8 bar. For all pressures, ignition temperatures increased with increasing turbulence intensity. A similar observation was made by Markides and Mastorakos [13] in a study of hydrogen autoignition in a turbulent co-flow of heated air with temperatures up to 1015 K at atmospheric pressure. The autoignition delay time increased with increasing air velocity at constant temperature, which they related to the increased turbulence intensity. In a recent computational study [14], Echekki and Gupta simulated the autoignition of a turbulent hydrogen jet in a hot co-flow and found that the ignition delay was longer than would be expected for homogeneous autoingnition.

To account for such effects in the context of gas turbine premixers, Beerer and McDonell [15] suggest the use of ignition delay times derived from flow reactor studies, since they better reflect the relevant fluid mechanics. Such experiments were carried out by e. g. Peschke and Spadaccini [16], Mueller et al. [17] and Beerer and McDonell [15]. However, since the air was electrically preheated, the initial flow reactor temperatures were limited to roughly 1000 K. Such studies therefore cannot address temperatures greater than 1000 K, which are relevant for reheat combustors. Furthermore, these studies were performed with electrically heated air, while practical reheat combustors inject fuel into hot exhaust gas. Since the gas composition affects the ignition delay [18, 19], it is necessary to investigate H_2 autoignition in cases where the fuel is injected into hot combustion products.

The purpose of the present study was to investigate autoignition of H_2 diluted with N_2 at reheat combustor relevant temperatures (> 1000 K), pressure (15 bar), and gas composition, with relevant residence times in the mixing zone. The experiments were performed in a generic, optically accessible reheat combustor [20] using high-speed imaging and Particle Image Velocimetry (PIV). Autoignition limits derived from parameter variations (temperature, velocity, fuel dilution) are presented and the nature of the autoignition events is discussed.

EXPERIMENTAL SET-UP

Research combustor

The experiments were performed in an optically accessible reheat combustor, which is illustrated schematically in Figure 1. It consists of three main sections. A hot gas generator (HG) generates hot flue gas at temperatures and compositions that are typical for practical reheat combustors. In the subsequent mixing section (MS), fuel is injected into the hot flue gas. The mixture is then burned in the subsequent reheat combustion chamber.

In the hot gas generator, a slightly modified FLOX® burner [21] was operated with NG at fuel lean conditions at a maximum thermal power of 590 kW. The exhaust gas of the burner was diluted with cold air to obtain a hot gas temperature and oxygen content typical for the inlet conditions of a reheat combustor mixing section.

The mixing section is comprised of a 25 x 25 mm square duct equipped with large quartz glass windows on each side. When

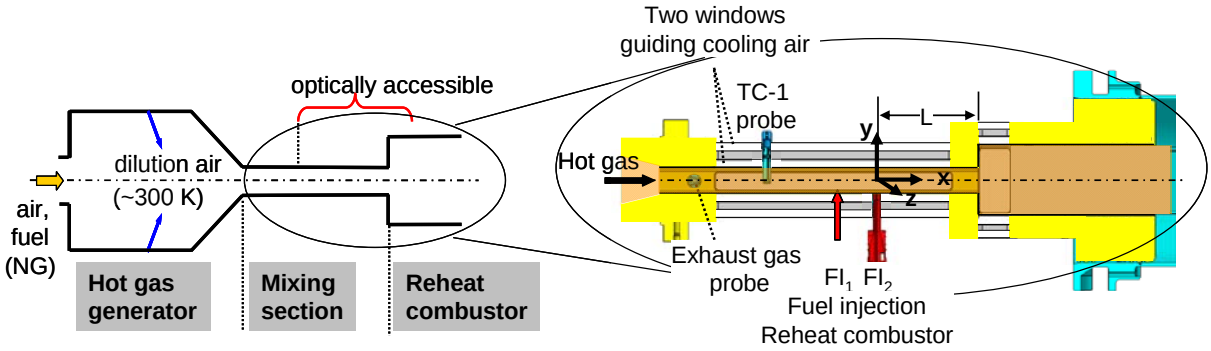

Figure 1: Reheat combustor

inserted into the employed high-pressure test rig, the field of view in the MS ranges from approximately 3 mm downstream of FI_1 (see Figure 1) to 26 mm upstream of the reheat combustion chamber in the x-direction, and ± 9 mm in the y- and z-directions. The reheat fuel is injected as a jet-in-crossflow from the lower wall, representing one single injection point of a multiple point fuel injector that is typically used in gas turbine combustors. The residence times in the MS are typical for the practical system. For the experiments described in this paper, the fuel injector was mounted in the more downstream position (FI_2 in Figure 1) of the two possible axial fuel injector positions, with a distance of L to the reheat combustion chamber. The fuel injector diameter was 5.6 mm.

The entrance to the reheat combustion chamber occurs as a sudden expansion, with a cross-sectional jump to 70 x 70 mm. In cases for which a reactive fuel/hot flue gas mixture entered the combustion chamber without autoigniting in the mixing section, the mixture autoignited at the combustor inlet and a flame stabilized in the reheat combustion chamber due to the outer recirculation zones. Quartz glass windows at all four sides of the combustion chamber allowed the flame root region to be observed.

Air- and watercooling systems designed for minimum combustor heat loss were used to cool the combustor walls. In the MS, only the metal parts were water-cooled. These parts were coated with a zirconium-oxide thermal barrier coating, resulting in a relatively low overall heat loss of about 6%.

The MS of the reheat combustor has been carefully characterized with respect to the temperature and velocity fields, as well as flue gas composition at the MS inlet [20]. The investigations revealed sufficient temperature homogeneity and a smooth velocity field. Furthermore, exhaust gas measurements have shown extremely low emission levels. Hence, the research combustor provides the required well-defined boundary conditions with respect to temperature and flue gas composition for an autoigniton study.

Operating conditions

The experiments were carried out at a pressure of p_{MS} = 15 bar and a flue gas oxygen content of around 15 vol. % at the MS inlet. Baseline MS inlet operating conditions (BL-H_2) were defined at a particular hot flue gas temperature $T_{MS} = T_{BL\text{-}H2} > 1000$ K and velocity $u_{MS} = u_{BL\text{-}H2} > 150$ m/s, leading to reheat combustor relevant residence times in the MS. These two parameters were varied with respect to the baseline values according to Table 1. The default fluid that was issued from the fuel injector was comprised of fuel and a carrier medium. For most operating conditions, the fuel consisted of H_2 and N_2 in a ratio of 80/20 vol. %, which will be referred to as the "80/20" case. At some operating conditions, a fuel composition of 70/30 vol. % ("70/30") was used to achieve different overall dilution and jet penetration depth. The equivalence ratio was $\Phi = 0.4$, resulting in a maximum thermal load of 890 kW and maximum momentum flux ratios of J = 2.6 (80/20) and J = 5.0 (70/30). However, autoignition often occurred at lower H_2 concentrations, as will be discussed in the section "Results and Discussion".

Table 1: Parameter matrix

Test case	u_{MS}	T_{MS}
A = BL-H_2	$u_{BL\text{-}H2} > 150$ m/s	$T_{BL\text{-}H2} > 1000$ K
B	$u_{BL\text{-}H2}$	$T_{low} = 0.975 \times T_{BL\text{-}H2}$
C	$u_{medium} = 1.25 \times u_{BL\text{-}H2}$	$T_{BL\text{-}H2}$
D	$u_{high} = 1.5 \times u_{BL\text{-}H2}$	$T_{BL\text{-}H2}$
E	u_{high}	$T_{high} = 1.025 \times T_{BL\text{-}H2}$
F	u_{high}	T_{low}

As in the practical system, a carrier medium was added to the fuel to achieve a greater jet penetration depth [22]. In this study, the carrier medium was N_2 that was perfectly premixed with the fuel (H_2 and fuel N_2) before injection to allow for mixing studies using planar laser-induced fluorescence (Tracer-PLIF). The carrier flow rate was such that the carrier-to-fuel mass flow ratio at the target operating point was unity. For the fuel composition of H_2/N_2 80/20 vol. %, the total composition of the jet (N_2 of the fuel plus carrier medium) injected into the

MS was $H_2/N_{2,total}$ = 64/36 vol. %. For the fuel composition of H_2/N_2 70/30 vol. %, it amounted to $H_2/N_{2,total}$ 51/49 vol. %. Often, autoignition occurred before these target operating points were achieved as described below. The temperature of the fuel/carrier mixture was between 298 and 318 K.

Measuring techniques

The temperature T_{MS} in the mixing section was measured with a single thermocouple (TC-1) probe at the axis of symmetry (y = 0 mm). It was permanently installed 110 mm upstream of the employed fuel injector position (FI_2) in the upper MS wall and was shielded with a ceramic casing to minimize radiative heat loss.

In order to visualize autoignition events in the MS, the broadband luminosity was recorded with two high-speed cameras (LaVision HSS5), one viewing from the side and one from the top. Light emission in the visible wavelength range (400 - 750 nm) was detected. Both cameras were mounted horizontally and a mirror was used to reflect the emitted light into the top-view camera. The cameras were equipped with commercial objective lenses (Nikkor). The side-view camera lens had a focal length of 85 mm and an f# of 1.4, while the top-view camera lens had a focal length of 135 mm and an f# of 2.0. Images were recorded at frame rates of 20, 25, and 30 kHz, depending on the conditions, with corresponding sensor resolutions of 896 x 160, 640 x 160 and 640 x 144 pixels. The cameras were operated in the post-triggering mode, in which images are taken continuously until a trigger signal is received. At the moment of triggering, images from about 0.5 s (depending on the recording rate and the special resolution) prior to and after the trigger signal were recorded. The trigger signal was initiated by the luminosity from autoignition events in the mixing section and was sufficiently responsive for the onset of autoignition and the subsequent development of the autoignition kernel to be reliably captured.

Particle Image Velocimetry (PIV) was used to measure the velocity field in the centerline plane (z = 0 mm) and in an off-centerline plane at z = -7 mm. The experimental set-up was similar to that described in Ref. [20], and only a brief description is provided here. A double-pulse dual cavity flashlamp-pumped Nd:YAG laser was triggered synchronously with a double frame CCD camera (LaVision ImagerProX) at a repetition rate of 15 Hz. The laser beam was expanded into an approximately 2 mm thick sheet and introduced into the MS through the top windows. TiO_2 particles with a nominal diameter of 1 µm were added to the dilution air, seeding the hot flue gas in the MS. The particle scattered light was recorded from the side. Velocity vectors were computed from the particle image cross-correlation using the LaVision DaVis 7 software package. A 16x16 pixel interrogation box was used, resulting in a spatial resolution of 1.6 mm. The velocity fields measured in the present experiment show good agreement to those from Ref. [20] under the same operating conditions.

The integral gas composition and emissions in the hot flue gas were measured with an exhaust gas probe with 3 gas inlets, mounted horizontally at the MS inlet. NO_x was measured via UV photometry (Limas 11), CO and CO_2 via IR photometry (Uras 14), and O_2 by paramagnetism (Magnos 16) at dry conditions. Unburned hydrocarbons (UHC) were measured with a flame ionization detector (Multi FID 14) at wet conditions.

Procedure and data analysis

The procedure for investigating autoignition limits involved several steps. At constant MS operation conditions (T_{MS}, u_{MS}) the reheat combustor fuel was injected as follows. First, the N_2 (N_2 of the fuel and the carrier medium) mass flow rates were adjusted to their set point values corresponding to the targeted fuel composition (H_2/N_2 80/20 or 70/30 vol. %, respectively) and Φ = 0.4. Then, the H_2 mass flow rate was incrementally increased towards its set point value, thereby increasing the H_2 concentration in the fuel in a stepwise manner. As soon as a flame stabilized in the mixing section, the high-speed cameras were triggered to capture the ignition event. The fuel was shut down a few seconds after a stable ignition event was observed to avoid damage due to thermal stresses.

The mixing section inlet pressure and temperature were measured at a rate of 1 Hz and a rise in both quantities was

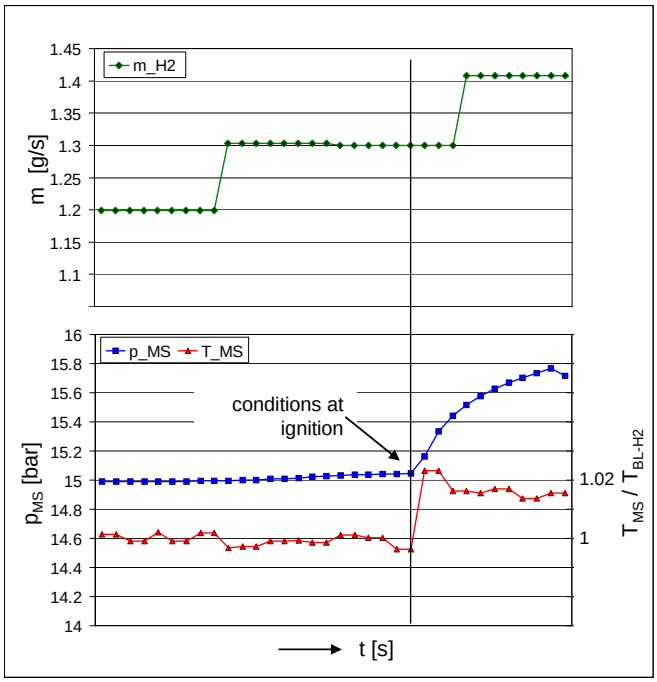

Figure 2: Example of a chronological sequence of the H_2 mass flow rate, temperature and pressure in the mixing section at ignition (black line). The data are logged every second.

observed during autoignition (see Figure 2). This is related to the thermal expansion and stronger penetration associated with the burning jet that occurred rapidly after the onset of autoignition [23]. To determine the conditions directly before ignition as accurately as possible, the ignition time was identified by a jump in temperature of $\Delta T > 0.005T_{MS}$ occurring simultaneously with a pressure jump of $\Delta p > 0.003p_{MS}$. The conditions (instantaneous T_{MS} and mass flow rates) at ignition were defined to be those at the measurement immediately prior the jumps in temperature and pressure (see Figure 2, black line). The instantaneous temperature at ignition differed from the design value of the respective operating point by a maximum of 1.6%. This deviation results from the day-to-day reproducibility and the operational standard deviation at steady conditions, both of which ranged up to 1%. In some cases the conditions could not be defined unambiguously, since for example the temperature increased in more then one step or the mass flow rate of H_2 was in a transient state. These cases were not considered for evaluating the autoignition limits.

RESULTS AND DISCUSSION

In the following, the H_2 concentration resulting in autoignition as a function of the MS boundary conditions will be described and discussed. Further, the nature of ignition kernels will be elucidated by looking at their development and the location of the first occurrence in relation to the mean velocity fields.

Autoignition limits

Table 2 summarizes the autoignition results, listing the mean H_2 concentrations in the fuel ($H_{2,fuel}$), in total (also considering the carrier medium ($H_{2,total}$)), the mean momentum flux ratio (J_{mean}), and the overall equivalence ratio (Φ_{mean}) at ignition for every operating point.

Table 2: Mean H_2 concentration in the fuel ($H_{2,fuel}$) and in the fuel/carrier mixture ($H_{2,total}$), mean momentum flux ratio (J_{mean}) and mean overall equivalence ratio (Φ_{mean}) at flame-stabilizing autoignition for every operating point (Test cases see Table 1).

Test case	reheat fuel	$H_{2,fuel}$	$H_{2,total}$	J_{mean}	Φ_{mean}
A	80/20	44	26	1.1	0.08
B1	80/20	54	34	1.3	0.12
B2	70/30	50	31	3.4	0.17
C	80/20	50	30	1.3	0.10
D1	80/20	66	46	1.7	0.19
D2	70/30	66	47	4.3	0.32
E1	80/20	50	31	1.3	0.10
E2	70/30	55	36	3.7	0.21
F1	80/20	Stable operation			
F2	70/30	Stable operation, except one autoignition event:			
		63	44	4.2	0.3

Figure 3 shows the influence of flue gas temperature in the mixing section on the maximum hydrogen concentration prior to an occurrence of autoignition. The temperature is normalized by the nominal baseline temperature, T_{BL-H2}. The y-axis shows the H_2 fuel concentration ($H_{2,fuel}$) in vol. %. In addition to the results from individual runs at a given operating point, the corresponding mean values for the cases with more than one run also are shown (black markers). The shaded lines illustrate the limits, below which generally no "flame-stabilizing autoignition kernels" occurred. The term "flame-stabilizing autoignition kernel" will be discussed in the next chapter. Cases at conditions A and B correspond to baseline MS inlet velocities, and conditions D-F correspond to 50% higher velocities (see Table 1).

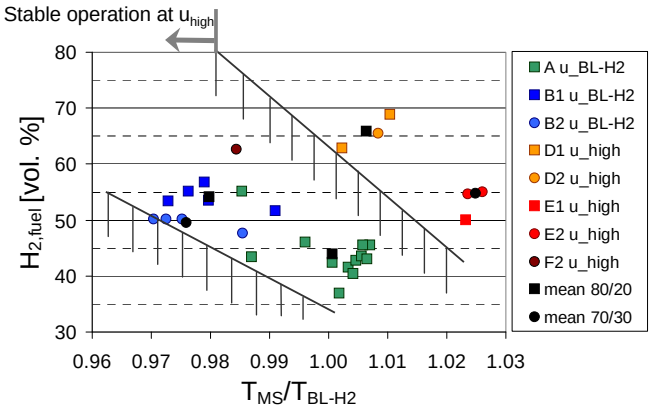

Figure 3: H_2 concentration in vol. % versus temperature T_{MS} in mixing section at flame-stabilizing autoignition, normalized by the nominal baseline temperature T_{BL-H2}.

Generally, the plot reveals a significant dependence of the H_2 concentration on temperature. At the baseline velocity, u_{BL-H2}, and a targeted fuel composition of H_2/N_2 80/20 vol. %, the maximum H_2 concentration before a flame-stabilizing autoignition kernel occurs increases by approximately 10% for a decrease in MS temperature of approximately 2% (cf. cases A and B1). The autoignition limits also are sensitive to the MS inlet velocity. For a higher velocity in the mixing section (cases D1and E1), an even greater increase in H_2 concentration (15%) can be achieved with the same temperature decrease of 2%. At the highest velocity (u_{high}) and lowest temperature (T_{low}) in the mixing section (case F1) stable reheat combustor operation can be achieved without the occurrence of a flame-stabilizing autoignition kernel in the MS. The results in Figure 3 show a steeper slope and hence a stronger temperature influence at higher velocities. This indicates that the dependence of the maximum H_2 fuel concentration on the temperature changes with velocity.

A fundamental parameter that influences whether autoigintion occurs is the ignition delay time relative to the residence time

of reactive mixtures in the MS. For residence times shorter than the ignition delay times, no autoignition can occur in the mixing section. Increasing the mixing section inlet velocity affects both of these properties. The ignition delay time is affected by the increased strain-rate between the flue gas and fuel, which alters both the flammability limits and the mixing rate, while the fluid residence time is decreased. Blouch and Law [12] reported that the turbulence level influences the dependence of the ignition temperature on the fuel concentration. In their study, the ignition temperature for a given fuel concentration increased with increasing turbulence intensity, which is consistent with the present results.

Considerable scatter in the H_2 concentration at autoignition for nearly corresponding temperatures can be observed in Figure 3. This is most likely related to the strong dependence of autoignition on the local history of temperature, mixture composition, and residence time of specific fluid parcels. The behavior of these fluid elements is influenced by random turbulent fluctuations as well as coherent vortex shedding and motion of the jet [10, 24]. Such random turbulent fluctuations might also explain the single ignition event at operating point F (u_{high}, T_{low}) and a targeted fuel composition of H_2/N_2 70/30 vol. %. Aside from this single event, stable and reproducible operation of the reheat combustor for about 1 hour was achieved at these operating conditions (cases F1, F2) for both H_2/N_2 mixtures (70/30 and 80/20 vol. %).

The target fuel composition was varied between 80/20 and 70/30 vol. % for the operating points B, D, E and F. This essentially equates to an increased N_2 flow rate as the H_2 is increased towards its target value, and hence greater penetration of the jet. It is noticeable that the ignition events for the series with a targeted H_2 concentration of 70/30 occurred at similar H_2 concentrations in the fuel as those for the series with an 80/20 target. Since the N_2 mass flow rates (N_2 dilution of the fuel and carrier N_2) were around 40% higher in the 70/30 series, similar H_2 concentrations in the fuel equates to considerably higher H_2 mass flow rates. This equates to an increase by a factor of roughly two in the overall equivalence ratios (Φ = 0.17 – 0.32 compared to 0.08 – 0.19) and momentum flux ratios (J = 3.4 – 4.3 compared to 1.1 – 1.7) at ignition for the 70/30 series compared to the 80/20 series. Hence, it can be concluded that the ignition is insensitive to the overall equivalence ratio. This is consistent with the shock tube study of Herzler et al. [5] at reheat combustor relevant temperatures and pressure, in which the H_2 ignition delay time was found to be almost independent of equivalence ratio. Furthermore, the present experimental results show that changes in the global mixing field due to momentum flux ratio changes do not influence the ignition behavior significantly. Autoignition is mainly controlled by the temporal histories of specific fluid elements, and the histories leading to autoignition do not appear to be strongly affected by the moderate changes in momentum flux ratio experienced here.

The H_2 concentration prior to the occurrence of a flame-stabilizing autoignition kernel also was plotted versus the velocity, normalized by the nominal baseline velocity. Figure 4 shows the results at T_{BL-H2}. Black symbols again indicate mean values and the shaded line illustrates the limit below which no flame-stabilizing autoignition kernels occurred.

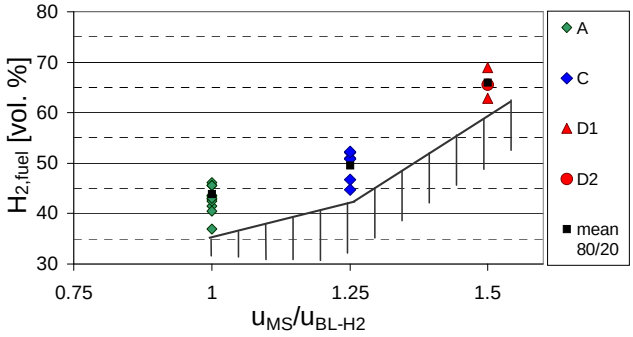

Figure 4: H_2 concentration in vol. % versus u_{MS} at flame-stabilizing autoignition for T_{BL-H2}, normalized by the nominal baseline velocity u_{BL-H2}.

This plot reveals a slightly non-linear dependence of the maximum H_2 fuel concentration without flame-stabilizing autoignition on velocity, and therefore on residence time. A velocity increase by 25% compared to u_{BL-H2} allows an increase of the maximum H_2 fuel concentration by 6%. A further velocity increase by another 25% led to a 16% higher maximum H_2 concentration in the fuel. Higher H_2 concentrations also equates to higher equivalence ratios, but as shown before this is not expected to influence the ignition behavior. Hence, the plot indicates a non-linear dependence of the maximum H_2 fuel concentration on the ignition delay time. Markides and Mastorakos [13] found ignition delay times to increase with increasing velocity at constant temperatures and atmospheric pressure. They related this to the increased turbulence intensity at higher velocities, which is consistent with the above observations.

Ignition kernel development

Having discussed the autoignition limits, the spatial and temporal development of ignition events will now be described in more detail. Analysis of the high-speed images shows that isolated ignition kernels often occurred that were convectively transported out of the MS, until eventually one kernel occurred in a region with particular conditions that allowed the kernel to ignite the entire fuel jet. A stable flame then formed that was anchored in the wake of the jet. Those events are classified as “flame-stabilizing autoingition kernels”. It was found that whether kernels ignited the main jet depended on the axial location at which they were formed, as will be discussed in more detail below.

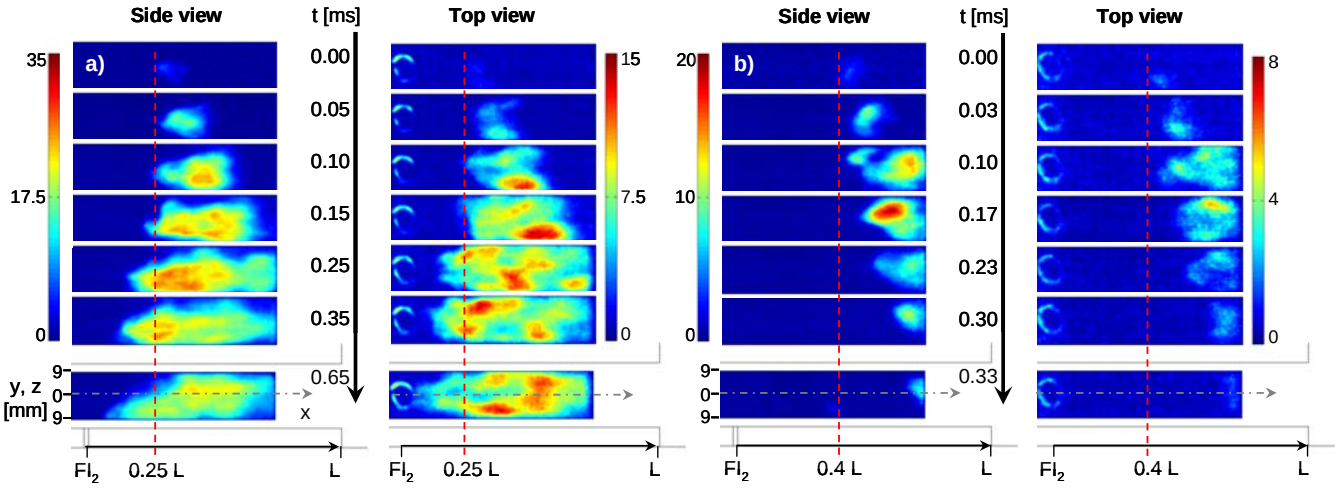

Figure 5: Single shot high-speed images (side and top view) extracted from two cases, one flame-stabilizing (a) and one non-stabilizing (b) ignition event (test case B2 and E2, respectively). Red lines indicate leading edge of the initial ignition kernel occurrence.

Figure 5 shows a sequence of instantaneous top- and side-view high-speed images extracted from two temporal series during which autoignition occurred. In case a), the kernel ignited a stable flame in the fuel jet, whereas in case b) the ignition kernel convected out of the MS. In the last image of each series, the walls of the MS and the cross-sectional jump to the reheat combustor are illustrated to clarify the geometry. The red lines mark the leading edge of the initial ignition kernel occurrence. The lower intensities in the top-view images are caused by the different camera objectives, the longer light path, and the mirror used with the top-view camera compared to the side-view camera (see section "Measuring techniques").

The ignition kernel resulting in a stable flame was recorded at operating conditions of test case B2 (H_2/N_2=70/30 vol. %, J = 3.4). The leading edge of the ignition kernel initially occurred at a location of x ≈ 0.25 L, near the axis of symmetry in the x-y-plane, and slightly off-center in the x-z plane. The kernel then increased in intensity and size in the streamwise (positive) axial direction and both positive and negative y- and z-directions, while the leading edge remained at roughly the same axial position (2^{nd} – 3^{rd} images). After the kernel spread over almost the entire channel height and width, it propagated upstream towards the fuel injector (4^{th} – 6^{th} images), thereby entering less mixed regions. This upstream propagation did not occur in the boundary layer where the lowest flow velocities are found, but might be promoted by the low axial velocity region in the jet wake. This issue will be considered further below. The flame occurred in highly stratified, partially premixed fluid, and very likely progressed upstream along the stoichiometric mixture fraction contour where the local flame speed is maximum. Finally, the flame stabilized near the fuel injector about 0.4 ms after the initial ignition kernel occurred (6^{th} – 7^{th} images).

A typical example of a non-stabilizing kernel (Figure 5b) was recorded at test case E (H_2/N_2=70/30 vol. %, J = 3.7). The initial ignition kernel occurred at x ≈ 0.4 L (leading edge), about 1 mm below the MS centerline in the y-direction and displaced by around -5 mm from the centerline in the z-direction. Similar to the previous case, the kernel then increased in intensity and size in the positive axial direction, positive and negative y- and z-directions, and spread over almost the entire MS width (2^{nd} – 3^{rd} images). However in this case, the leading edge was convectively transported downstream. The impression of an unchanged axial position of the leading edge is caused by another ignition kernel emerging at the upstream edge of the first kernel (3^{rd} images). Within the following 0.2 ms (4^{th} – 7^{th} images) the kernel was transported farther downstream, while still spreading over the entire MS width, until it almost exited the visible region of the MS (7^{th} images). In these 7^{th} images, another kernel occurring upstream in the MS can be observed. Such behavior was found in several high-speed sequences. One ignition kernel was formed, convected out of the MS, and was followed by one or several others. This series of kernels might be caused by local conditions that are favorable for autoignition at the same flow, jet, and MS inlet conditions that induced the first kernel. It could also be that the first kernel promotes changes in the MS conditions that promote further ignition events.

Ignition kernel location

The position of the first occurrence of each ignition kernel was determined from the side- and top-view high-speed images. The x-position is defined according to the leading edge of the kernel, extracted from the side-view image. The y- and z-positions are defined using the kernel centroid. For each operating condition, the initial position of every measured ignition kernel is plotted in Figure 6. Each marker shape represents one measurement sequence during which

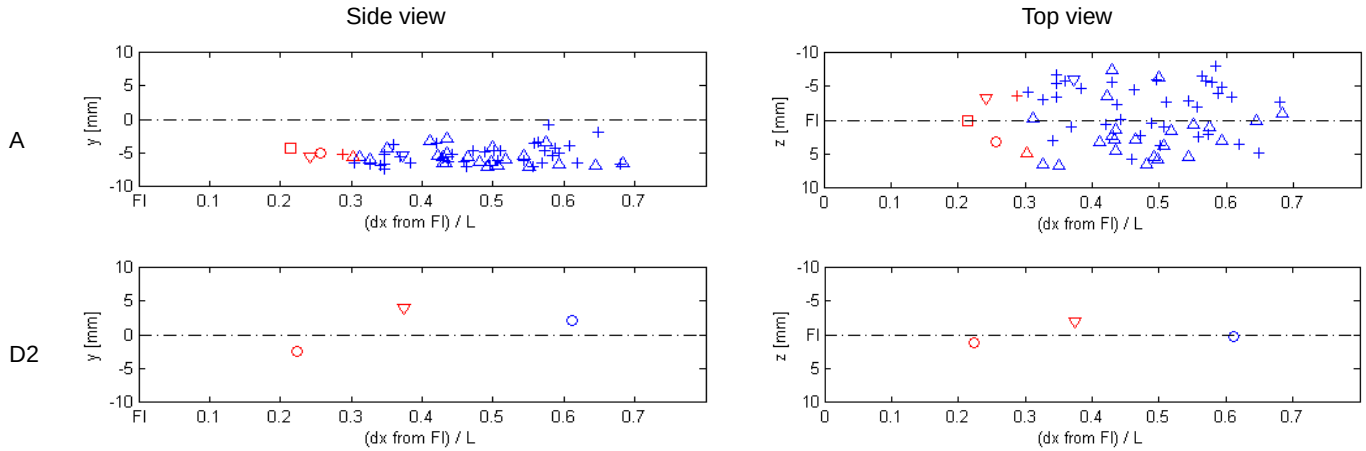

Figure 6: Typical plots for the positions of the first ignition kernel occurrence derived from the side and top-view high-speed images. Top line: A; bottom line: D2. Blue markers: non-stabilizing kernels, red markers: flame-stabilizing kernels.

autoignition occurred. Markers appearing multiple times in a single plot indicate that multiple ignition kernels occurred before one caused a stable flame. Kernels that did not cause stable flames are indicated by the blue markers, while those that did are indicated by red markers. Results from two typical conditions are provided, with the upper plots showing the ignition locations at baseline conditions (test case A, H_2/N_2=80/20 vol. %) and the lower plots showing a high velocity case (test case D, H_2/N_2=70/30 vol. %). From Figure 6, it is obvious that the flame-stabilizing and non-stabilizing kernels may be delineated by two distinct axial regions. This also is observed for the other test cases not shown here, with only a slight overlap of the two regions. At all operating conditions, the axial region in which flame-stabilizing kernels initially occurred covers the range of about 0.2 – 0.35 L, while non-stabilizing kernels initially appeared only at axial locations greater that approximately 0.30 L. The reason for this behavior will be discussed together with the velocity fields below.

The difference in the y-position of the kernels between the two test cases is obvious in the side-view images. In case A, all ignition events were located in the lower half of the MS, whereas in case D kernels also occurred above the MS centerline. This is representative of all 80/20 and the 70/30 test cases and is caused by the different momentum flux ratios, and hence the different jet penetration depths. In case A, the ignition kernels were spread over almost the entire visible width (z-direction) of the MS, indicating that the fuel was mixed over this width at the axial positions at which ignition occurred. When all high velocity cases (D-F, not all shown) are considered, ignition events also were found across the entire MS width.

For the high-velocity cases, the number of ignition kernels per flame-stabilizing autoignition event was lower than for the lower velocity cases (baseline A, B, medium velocity case C). However, the number of ignition kernels in the lower velocity cases varied strongly, from 1 to over 20 per flame-stabilizing autoignition event, for repetitions of the same operating point. This is likely related to fluctuating local and temporal conditions immediately before onset of ignition events, which cannot be resolved.

In order to help describe the flow properties leading to autoignition, velocity fields were measured at conditions similar to those at the autoignition limts. The velocity data were measured at baseline operating conditions (case A) and two different jet momentum flux ratios, which were similar to those in the autoignition measurements. The fuel mixtures used in the PIV study included additionally small amounts of natural gas (NG) to suppress autoignition [20]. To measure the velocity field representative for the autoignition cases with the targeted fuel composition of H_2/N_2 = 80/20 vol. %, a fuel composition $H_2/NG/N_2$ = 74/4/22 vol. % was used, resulting in Φ = 0.36 and a momentum flux ration of J = 1.5. This is only slightly different from the jet momentum in the autoignition measurements for the 80/20 cases, and therefore the same jet penetration and flow pattern are expected. In the PIV measurement representing the targeted fuel compositions of H_2/N_2 = 70/30 vol. %, a fuel composition of $H_2/NG/N_2$ = 62/8/30 vol. % with a carrier-to-fuel mass flow ratio of 1.5 was used. This results in Φ = 0.36 and J = 3.5, which was similar to the jet momentum in the autoignition measurements of case B2.

Figure 7 illustrates the mean and rms axial velocity fields normalized by the baseline velocity u_{BL-H2}, measured in the centerline (z = 0 mm) and off-centerline (z = -7 mm) planes for the two different jet compositions. The same color scaling is used for all axial and rms velocities. The black lines visualize the axial position of the fuel injector and the red lines illustrate the region in which the flame-stabilizing ignition kernels

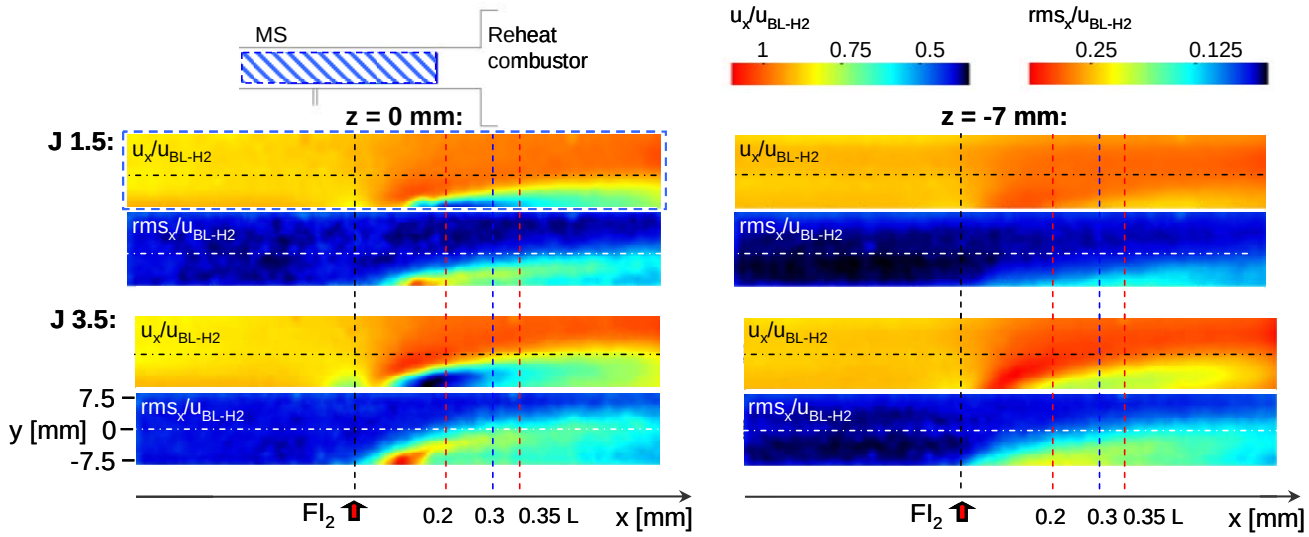

Figure 7: Axial mean and axial rms velocities measured at the z = 0 mm and z = -7 mm planes for H_2/NG/N_2 = 74/4/22 vol. % (J = 1.5) and H_2/NG/N_2 = 62/8/30 vol. % (J = 3.5), normalized by u_{BL-H2}. Black lines: axial position of the fuel injector, red lines: region in which the flame-stabilizing ignition kernels occurred, blue lines: downstream of these lines the non-stabilizing kernels were located.

occurred. Non-stabilizing kernels were located only downstream of the blue line.

Both cases exhibit the typical flow pattern of a jet-in-crossflow configuration [25], which is more pronounced in the centerline plane but still visible in the off-centerline plane. The axial velocity plots show that the main flow was deflected upwards and hence accelerated immediately upstream of the jet, leading to a low velocity region in the jet wake. For H_2/NG/N_2 74/4/22 (J = 1.5), the region with the lowest velocities, below about $0.5u_{BL-H2}$ (colored blue), was located close to the lower border of the visible region. For the J = 3.5 case this region extended to higher y-positions, but remained below the MS centerline. At z = -7 mm, the low velocity region for J = 1.5 is hardly visible and is likely located below the viewable region of the MS. The low velocity wake at z = -7 mm is still visible for the J = 3.5 case, although it is less distinct than at z = 0 mm.

The axial position of the low velocity region in the jet wake ranged from approximately 0.1 L to 0.35 L for both the J = 1.5 and 3.5 cases . These low axial velocity regions overlap quite well with the axial locations of ignition kernels that resulted in a stable flame attached to the jet. Kernels that convected out of the mixing section were located in the higher axial velocity regions. It therefore is clear that the ability of an autoignition kernel to create a stable flame is dependent on the ratio of axial velocity to the flame speed at the location where the kernel occurs. In the jet wake, the local flame speed appears to be sufficiently high such that the flame propagates upstream and stabilizes near the fuel injector. The upstream propagation for the 80/20 cases with smaller J occurred close to or below the visible part of the MS because of the low y-position of the jet wake (see images in Ref. [20]). For the 70/30 cases, with the larger J, the propagation is more within the visible portion of the combustor due to the greater jet penetration.

In regions farther downstream, the kernels were convectively transported out of the MS due to higher local axial velocities, which are assumed to have exceeded the local flame speed. The slight overlap of the regions containing flame-stabilizing and non-stabilizing ignition kernels is very likely related to fluctuations in the local velocity field. Similarly, the broad axial range where individual ignition kernels originated can be attributed to the different mixing, temperature, and velocity histories of different fluid parcels arising from the turbulence.

The rms velocity fluctuations in the main flow upstream of the fuel injector were up to $0.1u_{BL-H2}$. In the region of the jet, the rms fluctuations exceeded this value as the high velocity gradients in the shear layer led to enhanced turbulence production. For J = 1.5, the jet reached the MS centerline indicating an under-penetration, whereas for J = 3.5 it clearly crosses the centerline. The highest rms velocities are found in the jet wake directly behind the injector and are caused by the high vorticity in this region. Comparing the ignition kernel locations to the velocity fluctuation fields, the vertical kernel positions for the 80/20 and 70/30 operating points correspond to regions of high velocity fluctuations. For both cases, all ignition kernels were located downstream of the regions of the highest vorticity. Elevated rms velocities are also found in the off-centerline planes at axial positions very close to the fuel injector, indicating that the jet spreads over at least z = +/- 7 mm (on both sides due to symmetry). This also corresponds

to the ignition kernel locations, which spread over the visible MS width.

SUMMARY AND CONCLUSIONS

The autoignition of highly reactive fuels has been studied in a reheat combustor at operating conditions that are relevant to practical systems (p = 15 bar, T > 1000 K, hot flue gas, relevant residence times). The experiments were carried out in a generic, optically accessible reheat combustor using high-speed imaging and PIV. A perfectly mixed H_2/N_2 fuel jet was injected into a crossflow of hot flue gas in the mixing section of the reheat combustor. The minimum H_2 concentration leading to autoignition was determined by slowly increasing the H_2 fuel mass flow rate until a flame-stabilizing autoignition kernel occurred, while keeping the other parameters in the mixing section constant. The autoignition events were recorded with two high-speed cameras. Thus, autoignition limits for different mixing section (temperature, velocity) and fuel jet (N_2 dilution) parameters were derived. Further, the temporal and spatial development of the ignition kernels were discussed in context with velocity fields measured using PIV.

It was found that temperature is the dominant factor influencing autoignition, with a stronger influence at higher velocities. A temperature increase of about 2% led to a reduction in the highest possible H_2 concentration of about 16 vol. % at the highest flue gas velocity in the mixing section. Additionally, a slightly non-linear dependence was found between the maximum H_2 fuel concentration without flame-stabilizing autoignition and the velocity. The ignition characteristics at similar H_2 concentrations for different nitrogen mass flow rates in the reheat fuel reveals that the ignition is independent of the global equivalence ratio and macro-mixing. At the highest velocity and lowest temperature in the mixing section, the reheat combustor could be operated without flame-stabilizing autoignition in the mixing section for both H_2 fuel concentrations (70 and 80 vol. %).

Two different types of autoignition events were observed. The so-called “flame-stabilizing kernels” were characterized by an initial autoignition pocket that grew in size and then propagated upstream until the whole fuel jet ignited and a flame stabilized near the fuel injector. The flame-stabilizing kernels occurred in an axial range of $x \approx 0.2 – 0.35$ L in the mixing section, corresponding to the low axial velocity region in the fuel jet wake. The flame stabilizing behavior of these kernels was likely due to this low velocity, which allowed the flame to propagate against the flow. The so-called “non-stabilizing kernels” occurred farther downstream in the mixing section ($x \approx 0.3 – 0.7$ L). These kernels ignited and subsequently were convectively transported out of the mixing section, disappearing rather quickly. The location of the non-stabilizing kernels coincided with a region of higher axial velocity.

ACKNOWLEDGMENTS

This work has been funded by ALSTOM Power Generation AG, EnBW Holding AG and the “Ministerium für Wissenschaft, Forschung und Kunst (MWK) Baden-Württemberg” which is gratefully acknowledged. The authors would also like to thank U. Prestel, K. Ferst, S. Peukert and M. Kapernaum for their technical support during the measurements.

REFERENCES

[1] Lieuwen, T., McDonell, V., Petersen, E. and Santavicca, D., 2008, "Fuel Flexibility Influences on Premixed Combustor Blowout, Flashback, Autoignition, and Stability," J. Eng. Gas Turbines Power, **130**, pp. 011506 1-10.

[2] Joos, F., Brunner, P., Schulte-Werning, B., Syed, K. and Eroglu, A., 1996, "Development of the Sequential Combustion System for the ABB GT24/GT26 Gas Turbine Family," ASME Paper No. 1996-GT-315.

[3] Güthe, F., Hellat, J. and Flohr, P., 2009, "The Reheat Concept: The Proven Pathway to Ultralow Emissions and High Efficiency and Flexibility," J. Eng. Gas Turbines Power, **131**, pp. 021503 1-7.

[4] Mittal, G., Sung, C. J., Fairweather, M., Tomlin, A. S., Griffiths, J. F. and Hughes, K. J., 2007, "Significance of the HO_2+CO Reaction During the Combustion of CO+H_2 Mixtures at High Pressures," Proc. Combust. Inst., **31**, pp. 419-427.

[5] Herzler, J. and Naumann, C., 2009, "Shock-Tube Study of the Ignition of Methane/Ethane/Hydrogen Mixtures with Hydrogen Contents from 0% to 100% at Different Pressures," Proc. Combust. Inst., **32**(1), pp. 213-220.

[6] Keromnes, A., Donohoe, N., Curran, H., Herzler, J., Naumann, C. and Griebel, P., 2010, "Ignition Delay Time Measurements and Validation of Reaction Mechanism for Hydrogen at Gas Turbine Relevant Conditions," The Future of Gas Turbine Technology 5th International Conference, 27-28 October 2010, Brussels, Belgium, Paper No. 86.

[7] Lieuwen, T., McDonell, V., Santavicca, D. and Sattelmayer, T., 2008, "Burner Development and Operability Issues Associated with Steady Flowing Syngas Fired Combustors," Combust. Sci. Tech., **180**, pp. 1167-1190.

[8] Beerer, D., McDonell, V., Samuelsen, S. and Angello, L., 2009, "Interpretation of Flow Reactor Based Ignition Delay Measurements," ASME Paper No. GT2009-60268.

[9] Kreutz, T. G. and Law, C. K., 1996, "Ignition in Nonpremixed Counterflowing Hydrogen versus Heated Air: Computational Study with Detailed Chemistry," Combust. Flame, **104**, pp. 157-175.

[10] Mastorakos, E., 2009, "Ignition of Turbulent Non-Premixed Flames," Prog. Energy Combust. Sci., **35**, pp. 57-97.

[11] Fotache, C. G., Kreutz, T., Zhu, D. L. and Law, C. K., 1995, "An Experimental Study of Ignition in Nonpremixed

Counterflowing Hydrogen versus Heated Air," Combust. Sci. Tech., **109**, pp. 373-393.
[12] Blouch, J. D. and Law, C. K., 2003, "Effects of Turbulence on Nonpremixed Ignition of Hydrogen in Heated Counterflow," Combust. Flame, **132**, pp. 512-522.
[13] Markides, C. N. and Mastorakos, E., 2005, "An Experimental Study of Hydrogen Autoignition in a Turbulent Co-Flow of Heated Air," Proc. Combust. Inst., **30**, pp. 883-891.
[14] Echekki, T. and Gupta, K. G., 2009, "Hydrogen Autoignition in a Turbulent Jet with Preheated Co-Flow Air," Int. J. Hydrogen Energy, **34**, pp. 8352-8377.
[15] Beerer, D. J. and McDonell, V. G., 2008, "Autoignition of Hydrogen and Air Inside a Continuous Flow Reactor with Application to Lean Premixed Combustion," J. Eng. Gas Turbines Power, **130**, pp. 051507 1-8.
[16] Peschke, W. T. and Spadaccini, L. J., 1985, "Determination of Autoignition and Flame Speed Characteristics of Coal Gases Having Medium Heating Values," Research Project No. 2357-1, Report No. AP-4291.
[17] Mueller, M. A., Kim, T. J., Yetter, R. A. and Dryer, F. L., 1999, "Flow Reactor Studies and Kinetic Modeling of the H_2/O_2 Reaction," Int. J. Chem. Kinet., **31**(2), pp. 113-125.
[18] Riccius, O., Smith, R., Güthe, F. and Flohr, P., 2005, "The GT24/26 Combustion Technology and High Hydrocarbon ("C2+") Fuels," ASME Paper No. GT2005-68799.
[19] Lee, D. L., Yoo, C. S., Chen, J. H. and Frank, J. H., 2009, "Effects of H_2O and NO on the Extinction and Re-Ignition of Vortex-Perturbed Hydrogen Counterflow Flames," Proc. Combust. Inst., **32**, pp. 1059-1066.
[20] Fleck, J. M., Griebel, P., Steinberg, A. M., Stöhr, M., Aigner, M. and Ciani, A., 2010, "Experimental Investigation of a Generic, Fuel Flexible Reheat Combustor at Gas Turbine Relevant Operating Conditions," ASME Paper No. GT2010-22722.
[21] Lückerath, R., Meier, W. and Aigner, M., 2008, "FLOX® Combustion at High Pressure with Different Fuel Compositions," J. Eng. Gas Turbines Power, **130**, pp. 011505 1-7.
[22] Döbbeling, K., Hellat, J. and Koch, H., 2007, "25 Years of BBC/ABB/Alstom Lean Premix Combustion Technologies," J. Eng. Gas Turbines Power, **129**, pp. 2-12.
[23] Mörtberg, M., Blasiak, W. and Gupta, A. K., 2007, "Experimental Investigation of Flow Phenomena of a Single Fuel Jet in Cross-Flow During Highly Preheated Air Combustion Conditions," J. Eng. Gas Turbines Power, **129**, pp. 556-564.
[24] Rivero, A., Ferré, J. A. and Giralt, F., 2001, "Organized Motions in a Jet in Crossflow," J. Fluid Mech., **444**, pp. 117-149.
[25] Fric, T. F. and Roshko, A., 1994, "Vortical Structure in the Wake of a Transverse Jet," J. Fluid Mech., **279**, pp. 1-47.

